Submitted to: International Journal of Hydrogen Energy (**HE-D-13-03747**)
Date: March 6, 2014

Photocatalytic hydrogen generation with simultaneous organic degradation by composite CdS-ZnS nanoparticles under visible light

Xi Wang[1,2], Wen-chao Peng[2] and Xiao-yan Li[2]*

[1] School of Chemistry and Environment, South China Normal University, Guangzhou, Guangdong, China

[2] Environmental Engineering Research Centre, Department of Civil Engineering, The University of Hong Kong, Pokfulam Road, Hong Kong

(*Corresponding author: phone: 852 2859-2659; fax: 852 2859-5337; e-mail: xlia@hkucc.hku.hk)

Abstract

A visible light-driven CdS-ZnS photocatalyst in the form of nanoparticles with a heterogeneous structure was synthesized using the stepped microemulsion method. The composite CdS-ZnS was capable of simultaneous photocatalytic hydrogen production and organic degradation under visible light. The ZnS deposition on CdS helped suppress the recombination of electron/hole pairs generated on the more reactive CdS, leading to faster hydrogen production and improved stability of the CdS-ZnS in comparison to the bare CdS catalyst. Deposition of Ru on the catalyst surface further increased its photo-reactivity by about 4 times for hydrogen production. The heterostructured nanoparticles were effective in photocatalytic hydrogen production together with the degradation of model organic substances, including formic acid, methanol, and ethanol. The highest hydrogen production

rate was achieved by the (CdS-ZnS)/Ru catalyst at 266 mmol/m^2-h in the formic acid solution with an energy conversion efficiency of 3.05% in visible light, and the corresponding organic degradation rate in terms of the removal of chemical oxygen demand (COD) was estimated at 4272 mg COD/m^2-h.

Keywords: Hydrogen production, organic photolysis, CdS-ZnS, photocatalyst, visible light, solar energy.

Introduction

Hydrogen is one of the most promising clean and renewable energy carriers. It has a high combustion value and a near-zero level of pollutant and greenhouse gas emissions. Photocatalytic hydrogen generation from water is an attractive and environmentally-friendly method to harvest the solar energy [1]. However, while visible light (λ>420 nm) covers a large portion of the solar spectrum, most photocatalysts, such as TiO_2, function only under the energy-intensive UV light. Efforts have been made to develop novel photocatalysts, such as metal oxides (e.g. ZnO) and metal sulfides (e.g. CdS), that response to both UV and visible lights for water photolysis and hydrogen production [2, 3]. However, the solar energy conversion efficiency of these photocatalysts for hydrogen generation is still rather low due to mainly the recombination of photo-generated electron/hole pairs [4]. Moreover, an increase in reactivity of the photocatalyst would often result in a decrease in stability of the catalyst, leading to a rapid loss of its catalytic capability to photo-corrosion [5].

A well-structured co-catalyst that integrates the functions from two or more catalyst materials may offer solutions to the above problems. A highly photo-sensitive material with a narrow band gap, such as CdS, will provide a great photo-reactivity for H_2 generation, while the use of a relatively less active material with a wider band gap, such as ZnS, can effectively

reduce the electron/hole recombination and thereby protect the more active catalyst during the photocatalytic process [6]. In addition to hydrogen evolution (H^+ reduction), the photocatalytic reactions in water also render a strong oxidation power that may be utilized for wastewater treatment. In fact, photocatalytic oxidation has been developed as an advanced oxidation technology for treatment and pre-treatment of various pollutants in wastewater [7]. During the photocatalysis under solar light, model organic pollutants such as alcohols can function as electron donors for hydrogen evolution, whilst the organics are degraded [8, 9]. In such a photocatalytic application, both the purposes of hydrogen production and wastewater treatment can be achieved using the solar energy [5, 7].

CdS and ZnS are known as photocatalysts owing to their high photo-sensitivities [10, 11]. In addition to a sole catalyst material, research has been carried out to integrate CdS and ZnS or with other co-catalysts to increase the photo-reactivity of the catalysts [12-16]. However, most of the material integration was achieved in the form of a homogeneous system, e.g., a solid solution, which would only tailor the band gaps of the two catalyst materials [12-16]. In the present study, a composite CdS-ZnS catalyst with a heterogeneous structure was synthesized. The heterostructured catalyst was shown as a visible light-driven photocatalyst with a much improved photo-reactivity and photo-stability. A number of model organic substances were tested as electron donors for hydrogen production. The aim of the study was to achieve both photocatalytic hydrogen generation and organic wastewater treatment under visible light.

Materials and Methods

Synthesis of the CdS-ZnS catalysts

The stepped microemulsion technique was used to synthesize CdS-ZnS photocatalyst

nanoparticles with a heterogeneous structure. The synthesis was conducted in a water/Triton X-100/1-butanol/n-hexane system, with cadmium nitrate ($Cd(NO_3)_2$, 99%, Sigma-Aldrich) and zinc nitrate ($Zn(NO_3)_2$, 99%, Sigma-Aldrich) used as the Cd and Zn precursors, respectively, and sodium sulfide ($Na_2S \cdot xH_2O$, Sigma-Aldrich) as the S^{2-} source. To form the CdS nanoparticles, 40 ml of 0.1 M $Cd(NO_3)_2$ was placed in the microemulsion (W/O) solution and 50 ml of 0.1 M Na_2S was added dropwise under a vigorous stirring condition. The mixture was stirred for 15 min and 10 ml 0.1 M $Zn(NO_3)_2$ was then added to react with excess S^{2-} to form ZnS that deposited on CdS particles. The mixture was stirred for 6 h at room temperature. A Cd to Zn precursor ratio of 0.8 to 0.2 was used for the microemulsion process to form $(CdS)_{0.8}/(ZnS)_{0.2}$. The CdS-ZnS solid precipitates formed in the solution were centrifuged and washed with DI water and alcohol. For comparison, a homogeneous solid solution of $Cd_xZn_{1-x}S$ with a Cd to Zn ratio of 0.8:0.2 was also prepared using the one-step microemulsion method. A pre-determined amount of 0.1 M $Cd(NO_3)_2$ and a pre-determined amount of 0.1 M $Zn(NO_3)_2$ were mixed together and placed in the microemulsion (W/O) solution. An excessive amount of 0.1 M Na_2S was added drop-wise to the W/O liquor to form the precipitates of $Cd_{0.8}Zn_{0.2}S$ under a vigorous stirring condition. Similarly, the solid particles were recovered and washed. The dry catalyst powder obtained from each batch was annealed at 723 K in a furnace (LHT 02/16 LBR, Nabertherm) supplied with pure nitrogen for 2 hr. Afterward, the powder was grounded by ball mill for 5 min and then stored in dark before use.

Ruthenium (Ru) was deposited on the surface of the catalyst using *in-situ* photo-deposition in an acetic acid solution of $RuCl_3$ (Aldrich). Photo-deposition was carried out by illuminating (λ>420 nm, 300 W Xe lamp) the CdS-ZnS catalyst particles suspended in the $RuCl_3$ solution for 20 min. The load of Ru coating was around 5% of the CdS-ZnS content, and the resulting composite catalyst was denoted as (CdS-ZnS)/Ru.

Characterization of the photocatalysts

The size distribution of the catalyst particles was measured by a laser diffraction particle size analyzer (Delsa™ Nano, Beckman Coulter). The BET surface area of the photocatalyst was determined by a surface area analyzer (SA3100, Beckman Coulter). The diffuse reflection spectrum (DRS) of the photocatalyst was obtained using a UV-vis spectrophotometer (Lambda 25, Perkin Elmer) that was converted from the reflection function to the absorbance function following the Kubelka-Munk method [17]. The crystalline phases and structural features of the catalysts were analyzed by an X-ray diffraction (XRD) system (D8 Advance, Burker AXS) with the Cu Kα irradiation from 10 to 90 degrees. The morphology of the catalyst particles was examined and their selected area electron diffraction (SAED) pattern was obtained using a transmission electron microscope (TEM) (Tecnai G2 20 S-TWIN, Philips FEI). In addition, the TEM equipped with an energy-dispersion spectroscopy (EDS) was employed to obtain the element mapping distribution for the photocatalyst.

Photocatalytic H_2 production in different model organic solutions under visible light

The photocatalytic hydrogen production experiments were conducted in a circular photo cell made of Pyrex class with a quartz window on the top. A 300 W Xe lamp (wavelength 250-750 nm) was used in a light source setup (PLS-SXE, Trustech) to simulate the solar light. A cutoff ($\lambda < 420$ nm) filter was installed to yield only visible light (light intensity ~ 70 mW/cm^2 measured by a light power meter, I400, Trustech) over a lighting area of 33 cm^2 from the top of the photo cell. A certain amount of the photocatalyst, i.e. 0.15 g of the CdS-ZnS or (CdS-ZnS)/Ru powder, was suspended in 150 mL of water or an organic solution.

Different model organic compounds, including formic acid, methanol and ethanol, were tested as electron donors for photocatalytic hydrogen production. The solution had an organic content of 10% and was kept at pH~7. The gas produced during the photo-tests was collected, and the H_2 and CO_2 contents were analyzed by a gas chromatograph (GC HP5890 Series II, Hewlett Packard). Each run of the photo-test lasted for around 4 hrs. The H_2 production rate for a test was calculated from the slope of the linear regression of the accumulated hydrogen production vs. time. Each test was repeated at least once, and the average results are reported for the duplicate. The reactivity of the photocatalyst was evaluated in terms of the specific hydrogen production rate (R) and the energy conversion efficiency (η), as described by the following equations:

$$R_A = \frac{\Delta m_{H_2}}{A\Delta t}, \text{ or} \quad (1)$$

$$R_A = \frac{\Delta m_{H_2}}{W\Delta t}, \text{ and} \quad (2)$$

$$\eta = \frac{R\ \Delta H_C}{I} \quad (3)$$

where R_A and R_w are the area-based and weight-based specific hydrogen production rates, respectively, Δm_{H2} is the moles of H_2 production measured, Δt the duration of the photo-reaction, A the irradiation area (33 cm^2), W is the amount (weight) of the catalyst in the photo cell, ΔH_c is the combustion value of H_2 (286 kJ/mol) and I the light density. The hydrogen production rates reported below were normally obtained from the first 2 or 3 test runs for the newly prepared photocatalysts.

The quantum yield (QY) of the photocatalytic reaction was also calculated as follows, which has been used to evaluate the reactivity of a photocatalyst for H_2 production under light irradiation over a broad band of wavelength,

$$QY = \frac{m_{re}}{m_{ip}} = \frac{2m_{H_2}}{m_{ip}} \quad (4)$$

where m_{re} is the amount of reacted electrons which is two times of the moles of H_2 produced (m_{H2}), and m_{ip} is the amount of total incident photons for the catalyst in the photo cell. The amount of incident photons for the setup of the photocatalytic tests was determined by the method of ferrioxalate actinometer employing potassium ferrioxalate ($K_3[Fe(C_2O_4)_3]$) [18].

To evaluate the reproducibility of the experiment and the stability of the catalyst, the photocatalytic hydrogen generation test was repeated for 10 times for each type of the catalysts. In addition, the amount of Cd^{2+} leaching into the solution during the photocatalytic experiments was measured by an atomic absorption spectrometer (AAnalyst 300, Perkin Elmer).

Results and Discussion

Characterization of the photocatalysts

The CdS-ZnS catalysts are nanoparticles that ranged from 40 to 340 nm with a number-based mean size of around 100 nm according to the particle size analysis. The TEM images show that the catalysts had primary particles of about 60 nm (Figure 1). Moreover, rather than a homogeneous solid solution, the CdS-ZnS catalysts synthesized by the two-step microemulsion process appeared to be of a heterogeneous structure with ZnS deposited on the surface of the CdS crystals (Figure 1A-C). According to the TEM-EDS mapping result, the composite catalysts were Cd-based nanoparticles with Zn distributing mostly on the particle surface (Figure 1D-F). Based on the SAED patterns given in Figure 2, the comparison between pure CdS and CdS-ZnS confirmed the presence of cubic phase ZnS (d-Spacing = 0.320 nm (111), 0.195 nm (220), 0.165 nm (222)) in the composite catalyst [19].

A good crystal phase of CdS can be found in the CdS-ZnS catalyst according to its XRD pattern (Figure 3). More specifically, the crystal structure of CdS-ZnS is dominated by the hexagonal CdS phase. Due to likely the low ZnS content in the CdS-ZnS particles, the peak of ZnS could not be clearly identified in the XRD spectra. A similar result has been previously reported for the CdS-ZnS catalyst by Soltani et al. [20]. For the solid solution of $Cd_{0.8}Zn_{0.2}S$, the diffraction peaks were found to shift to higher angles in comparison to CdS, which is consistent with previous findings [21]. In contrast, the heterostructured CdS-ZnS did not show such a shift of the diffraction peaks from those of CdS.

The diffuse reflection spectra of CdS-ZnS and its base materials (CdS and ZnS) are presented in Figure 4 to show the sensitivity of the photocatalysts to visible light. As expected, ZnS did not response to visible light, while CdS had an intensive absorption band in the visible region with a band gap of 2.23 eV. CdS-ZnS also responded well to visible light with a band gap of 2.31 eV, although it blue shifted slightly, which is consistent with the results of Soltani et al. [20]. The similar refection spectra between CdS and CdS-ZnS indicate that the photo-reactivity of CdS was well remained in the composite CdS-ZnS catalyst.

Photocatalytic hydrogen production by the CdS-ZnS catalyst under visible light

The CdS-ZnS nanoparticles were capable of photocatalytic hydrogen generation together with organic degradation under visible light (Figure 5A). Bare CdS had a hydrogen production rate of only 13.7±1.2 μmol/h in the formic acid solution, while ZnS was not able to produce hydrogen under visible light. In comparison, CdS-ZnS was shown as a much effective visible light-driven photocatalyst that could produce hydrogen at a rate of 189.5±3.5 μmol/h. Coating of ZnS on the CdS surface formed a heterogeneous nanoparticle structure, resulting in a significant increase of the hydrogen production activity of the photocatalyst. In

comparison, simply incorporating Zn into the CdS structure was not effective to enhance the photo-activity of the catalyst. The H_2 production rate by the structured CdS-ZnS ($(CdS)_{0.8}/(ZnS)_{0.2}$) was found to be about 10 times of that by the $Cd_{0.8}Zn_{0.2}S$ solid solution (180 vs. 18 mmol/m^2-h) in the S^{2-}/SO_3^{2-} solution under the same photocatalytic conditions.

The composite CdS-ZnS heterostructure apparently brought about a synergetic function of the catalyst materials. The use of the more photo-sensitive CdS ensured the reactivity of the photocatalyst [3], while the ZnS functioned to suppress the recombination of electron/hole pairs formed on CdS, making the electros more available for H^- reduction and H_2 evolution [8, 9]. Moreover, the use of the outer ZnS could help increase the stability of the CdS-based photocatalyst. After 10 runs of the photocatalytic tests, the CdS-ZnS catalyst still maintained 86% of its hydrogen productivity at a level of 166.0 μmol/h, whilst the bare CdS had only 46% of its reactivity remaining for hydrogen production at a low rate of 6.3 μmol/h (Figure 5B). The ZnS coating could also minimize the leaching of Cd^{2+} from the catalyst nanoparticles during the photocatalytic process. Between test runs 2 and 5, the CdS-ZnS catalyst had an average Cd^{2+} leaching rate of 68.5 μg/h, while the pure CdS particles had a high Cd^{2+} leaching rate of 334.6 μg/h. Between runs 6 and 10, the leaching of Cd^{2+} from the CdS-ZnS catalyst decreased to a much lower level at 9.5 μg/h, in comparison to bare CdS that had a Cd^{2+} leaching rate of 103.2 μg/h. Coating of ZnS could effectively protect the more reactive CdS catalyst and hence greatly improved its stability against photo-corrosion.

Photocatalytic hydrogen generation together with organic degradation by the CdS-ZnS catalysts

Deposition of ruthenium on the CdS-ZnS surface further enhanced the hydrogen productivity of the photocatalyst under visible light (Figure 6). With the Ru deposition on the

catalyst surface, the photocatalytic hydrogen production rate increased about 4 times. For both CdS-ZnS and (CdS-ZnS)/Ru in pure water, no hydrogen was produced in the absence of the model organics. The presence of organic enabled the catalyst to effect photocatalytic H_2 generation, as the model organics functioned as electron donors for the reduction of H^+ ions to realize hydrogen evolution.

The highest H_2 production rate was achieved with the (CdS-ZnS)/Ru catalyst at 266±4 mmol/m^2-h in formic acid with an overall energy conversion efficiency of 3.05±0.05 % and a quantum yield of around 20%. In water pollution control, the chemical oxygen demand (COD) is commonly used to measure the concentration of organic matter in water. In theory, COD is the amount of oxygen that would be consumed for organic oxidation. During the organic oxidation, electrons donate electrons that are accepted by oxygen, and every four moles of electrons donated by the organic matter correspond to one mole of oxygen consumed. During the photocatalytic process, oxidation (organic oxidation) and reduction (H^+ reduction) also occur simultaneously. The amount of electrons provided by the organic would be equal to the amount of electrons received by H^+ for H_2 evolution. Thus, theoretically, the amount of organic degradation in terms of COD removal can be estimated as follows in relation to the amount of H_2 production,

$$COD\ \ removal = \frac{m_{H_2} M_{O_2}}{2} \tag{5}$$

where M_{O_2} is the molar mass of O_2 (32 g/mol). The theoretical photocatalytic COD reduction rate for formic acid was 14.1 mg/h by the (CdS-ZnS)/Ru catalyst (Figure 7A), corresponding to an area-based specific rate of 4272 mg COD/m^2-h under visible light. Meanwhile, CO_2 was produced at a rate of 226 mmol/m^2-h in the gaseous phase during the photocatalytic test, which agrees well with the theoretical COD reduction rate. The molar ratio of hydrogen to carbon dioxide productions was approximately 1:1, suggesting a complete decomposition of

227 formic acid [22].

228 However, CO_2 production was not detected during the photocatalytic H_2 generation in
229 both methanol and ethanol solutions. It is likely that the photocatalytic reactions resulted in
230 organic degradation and intermediate formation other than complete organic mineralization
231 [8]. When the CdS-ZnS catalyst was excited by visible light, the photo-generated holes would
232 attack methanol or ethanol, leading to the following organic degradations [8, 23],

233 $$CH_3OH + h^+ \longrightarrow HCHO + H^+;$$

234 $$CH_3CH_2OH + h^+ \longrightarrow CH_3CHO + H^+.$$

235 The photocatalytic hydrogen production rates increased as the model organic
236 concentration in solution increased (Figure 5B). For formic acid in the concentration range of
237 0–10%, the H_2 production rate by CdS-ZnS increased linearly (r = 0.98) with the formic acid
238 concentration. Beyond the range (>10%), the H_2 production rate did not show a significant
239 increase with the formic acid concentration. For both methanol and ethanol, the
240 photocatalytic hydrogen production rate also increased nearly linearly with the organic
241 concentration. As the initial concentration decreased to a low level of 500 mg/L, hydrogen
242 still could be produced from methanol and ethanol at 12.3±2.5 and 9.6±2.0 mmol/m^2-h,
243 respectively. The specific hydrogen production rates based on the irradiation area or the
244 amount of catalyst were summarized in Figure 6. The hydrogen production rates in the
245 methanol and ethanol solutions were 220.9±5.2 mmol/m^2-h and 122.1±3.0 mmol/m^2-h,
246 respectively, which are more than 2.5 times higher than that reported by Zhang and Zhang [7]
247 for the Ru/CdS/Al-HMS catalyst under similar conditions (350 W Xe lamp). The quantum
248 efficiency of (CdS-ZnS)/Ru (20%) is more than an order of magnitude higher than that of
249 Ru/CdS/Al-HMS (1.2%) [7]. Hydrogen production in 10% methanol achieved a production
250 rate of 4.8±0.3 mmol/g-h for visible light irradiation, which is ten times of the specific

hydrogen production rate reported for the $CuO/Al_2O_3/TiO_2$ catalyst in 10% methanol under solar irradiation [24]. The higher hydrogen generation and organic degradation efficiency suggests the advantage of the heterostructure of the photocatalyst. Although ZnS cannot be excited directly by visible irradiation, the photo-sensitive CdS can be readily excited by visible light. With its excitation, CdS would function as a photo-sensitizer to induce the excitation of ZnS. The more negative conduction band (-1.4 V) of ZnS allows photo-excited electrons to drop to the conduction band of CdS (-0.3 V) [24] and the electron flow from ZnS to CdS supplies more electrons to the conduction band of CdS for transfer to the aqueous phase for H^+ reduction. Meanwhile, the holes left at the valance band of ZnS would attract electrons from the chemical solution, resulting in organic oxidation and degradation.

Conclusions

The composite CdS-ZnS nanoparticles with a heterogeneous structure were synthesized as a visible light-driven catalyst capable of both photocatalytic hydrogen production and organic degradation. The ZnS deposited on CdS would suppress the recombination of electron/hole pairs formed on CdS, leading to a faster hydrogen generation rate in comparison to bare CdS. The ZnS coating also helped protect the more sensitive CdS and hence greatly improve its stability against photo-corrosion. The presence of model organic substances, including formic acid, methanol and ethanol, enabled photocatalytic hydrogen production under visible light. The highest specific hydrogen production rate was achieved by the (CdS-ZnS)/Ru catalyst at 266±4 mmol/m^2-h in the formic acid solution with a photo energy conversion efficiency of 3.05±0.05%. In relation to the hydrogen production, the corresponding photocatalytic organic degradation rate was 4272±67 mg COD/m^2-h.

Acknowledgements

This research was supported by grant HKU714112E from the Research Grants Council (RGC) of the Government of Hong Kong SAR and project 51308230 from the National Natural Science Foundation of China (NSFC). The technical assistance of Mr. Keith C.H. Wong is highly appreciated.

References:

[1] Grimes C, Varghese OK, Ranjan S. Light, water, hydrogen: the solar generation of hydrogen by water photoelectrolysis. New York, USA: Springer; 2008.

[2] Bao NZ, Shen LM, Takata T, Domen K. Self-templated synthesis of nanoporous CdS nanostructures for highly efficient photocatalytic hydrogen production under visible light. Chem Mater 2008;20:110-7.

[3] Wang X, Shih K, Li XY. Photocatalytic hydrogen generation from water under visible light using core/shell nano-catalysts. Water Sci Technol 2010;61:2303-8.

[4] Lee MT, Werhahn M, Hwang DJ, Hotz N, Greif R, Poulikakos D, et al. Hydrogen production with a solar steam-methanol reformer and colloid nanocatalyst. Int J Hydrogen Energy 2010;35:118-26.

[5] Zong X, Yan HJ, Wu GP, Ma GJ, Wen FY, Wang L, et al. Enhancement of photocatalytic H_2 evolution on CdS by loading MoS_2 as cocatalyst under visible light irradiation. J Am Chem Soc 2008;130:7176-7.

[6] Yu ZG, Pryor CE, Lau WH, Berding MA, MacQueen DB. Core-shell nanorods for efficient photoelectrochemical hydrogen production. J Phys Chem B 2005;109:22913-9.

[7] Zhang YJ, Zhang L. Preparation of Ru-loaded CdS/Al-HMS nanocomposites and production of hydrogen by photocatalytic degradation of formic acid. Appl Surf Sci

2009;255:4863-6.

[8] Best JP, Dunstan DE. Nanotechnology for photolytic hydrogen production: colloidal anodic oxidation. Int J Hydrogen Energy 2009;34:7562-78.

[9] Cao YW, Banin U. Growth and properties of semiconductor core/shell nanocrystals with InAs cores. J Am Chem Soc 2000;122:9692-702.

[10] Reber JF, Meier K. Photochemical production of hydrogen with zinc-sulfide suspensions. J Phys Chem 1984;88:5903-13.

[11] Bao N, Shen L, Takata T, Domen K, Gupta A, Yanagisawa K, et al. Facile Cd-thiourea complex thermolysis synthesis of phase-controlled CdS nanocrystals for photocatalytic hydrogen production under visible light. J Phys Chem C 2007;111:17527-34.

[12] Kudo A, Sekizawa M. Photocatalytic H_2 evolution under visible light irradiation on $Zn_{1-x}Cu_xS$ solid solution. Catal Lett 1999;58:241-3.

[13] Li MT, Jiang JG, Guo LJ. Synthesis, characterization, and photoelectrochemical study of $Cd_{1-x}Znx_S$ solid solution thin films deposited by spray pyrolysis for water splitting. Int J Hydrogen Energy 2010;35:7036-42.

[14] Liu GJ, Zhao L, Ma LJ, Guo LJ. Photocatalytic H_2 evolution under visible light irradiation on a novel $Cd_xCu_yZn_{1-x-y}S$ catalyst. Catal Commun 2008;9:126-30.

[15] Priya R, Kanmani S. Solar photocatalytic generation of hydrogen under ultraviolet-visible light irradiation on (CdS/ZnS)/Ag_2S+(RuO_2/TiO_2) photocatalysts. Bull Mater Sci 2010;33:85-8.

[16] Tambwekar SV, Venugopal D, Subrahmanyam M. H_2 production of (CdS-ZnS)-TiO_2 supported photocatalytic system. Int J Hydrogen Energy 1999;24:957-63.

[17] Kubelka P, Munk F. Ein Beitrag zur Optik der Far- banstriche. Zeitschrift Technische Physik 1931;12:593-601.

[18] Montalti M, Murov SL. Handbook of Photochemistry. Boca Raton: CRC/Taylor &

Francis; 2006, 650 p.

[19] Dumbrava A, Badea C, Prodan G, Popovici I, Ciupina V. Zinc sulfide fine particles obtained at low temperature. Chalcogenide Letters 2009;6:437-43.

[20] Soltani N, Saion E, Yunus WMM, Erfani M, Navasery M, Bahmanrokh G, et al. Enhancement of visible light photocatalytic activity of ZnS and CdS nanoparticles based on organic and inorganic coating. Appl Surf Sci 2014;290:440-7.

[21] Zhang K, Jing DW, Xing CJ, Guo LJ. Significantly improved photocatalytic hydrogen production activity over $Cd_{1-x}Zn_xS$ photocatalysts prepared by a novel thermal sulfuration method. Int J Hydrogen Energy 2007;32:4685-91.

[22] Chen T, Wu G, Feng Z, Hu G, Su W, Ying P, et al. In situ FT-IR study of photocatalytic decomposition of formic acid to hydrogen on Pt/TiO_2 catalyst. Chinese J Catal 2008;29:105-7.

[23] Chiarello GL, Forni L, Selli E. Photocatalytic hydrogen production by liquid- and gas-phase reforming of CH_3OH over flame-made TiO_2 and Au/TiO_2. Catal Today 2009;144:69-74.

[24] Miwa T, Kaneco S, Katsumata H, Suzuki T, Ohta K, Verma SC, et al. Photocatalytic hydrogen production from aqueous methanol solution with $CuO/Al_2O_3/TiO_2$ nanocomposite. Int J Hydrogen Energy 2010;35:6554-60.

Figure captions:

Figure 1. TEM examination and EDS element mapping result of the CdS-ZnS catalyst: (A)-(C) TEM images showing the heterostructure of the catalyst particles, (D) TEM image for the EDS mapping of (E) Cd distribution and (F) Zn distribution.

Figure 2. The SAED pattern of (A) pure CdS and (B) the structured CdS-ZnS.

Figure 3. XRD spectra of the catalyst materials: the structured CdS-ZnS composite and pure CdS and ZnS.

Figure 4. Diffuse reflection spectra of the photocatalysts: the structured CdS-ZnS composite in comparison with pure CdS and ZnS.

Figure 5. (A) Hydrogen production in the formic acid solution (10%) by the composite CdS-ZnS, bare CdS and bare ZnS, under visible light; and (B) stability of CdS-ZnS and bare CdS in terms of the hydrogen production rate and leaching of Cd^{2+} from the catalysts during the repeated photocatalytic tests (at least 4 hr for each test cycle).

Figure 6. (A) The area-based and (B) weight-based specific hydrogen production rates of the photocatalysts of CdS-ZnS and (CdS-ZnS)/Ru in different model organic solutions under visible light.

Figure 7. (A) The theoretical COD removal rate by the CdS-ZnS and (CdS-ZnS)/Ru photocatalysts for different organic solutions under visible light; and (B) the effect of the initial organic concentration on the rate of photocatalytic hydrogen production by CdS-ZnS under visible light.

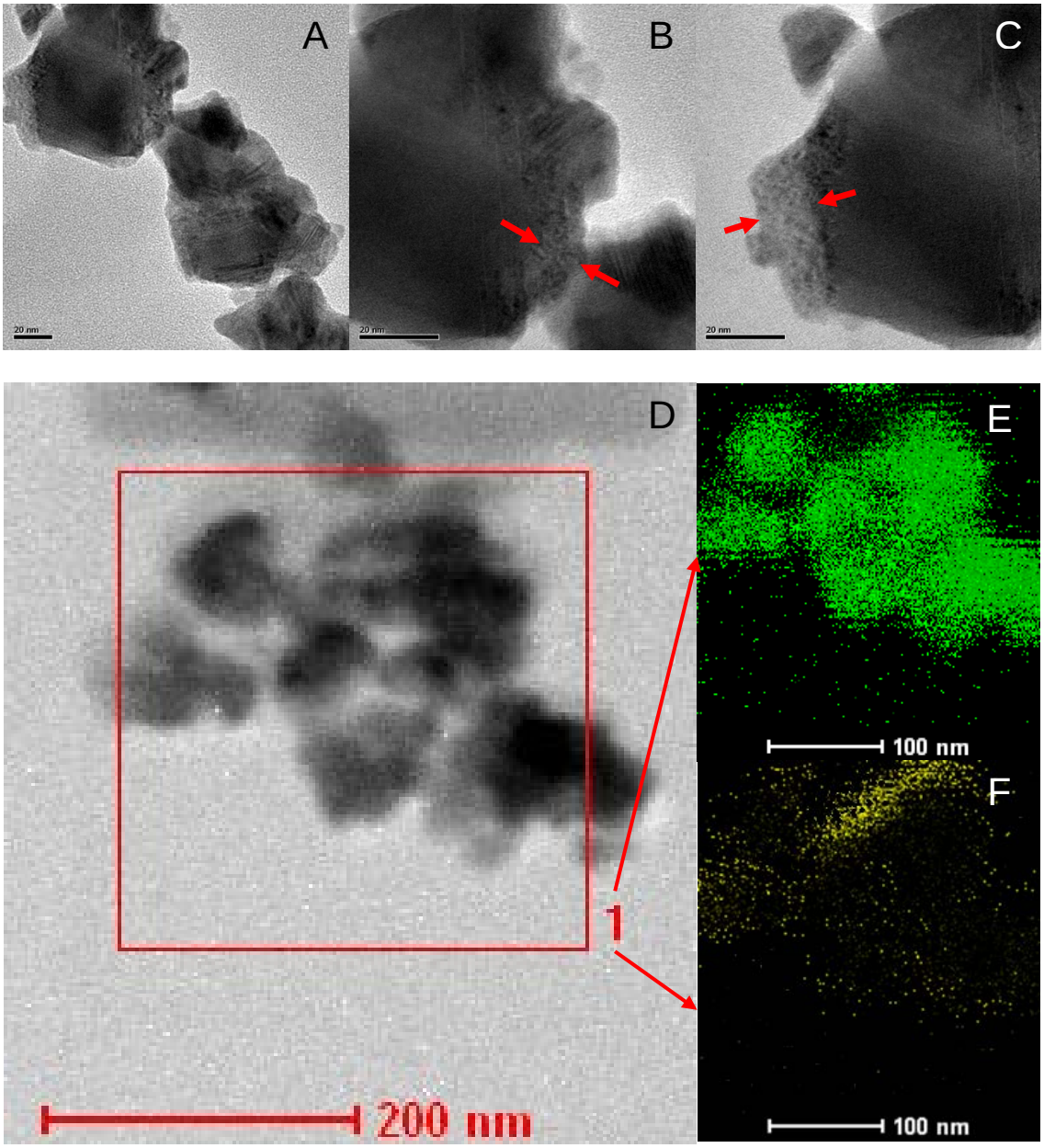

Figure 1. TEM examination and EDS element mapping result of the CdS-ZnS catalyst: (A)-(C) TEM images showing the heterostructure of the catalyst particles, (D) TEM image for the EDS mapping of (E) Cd distribution and (F) Zn distribution.

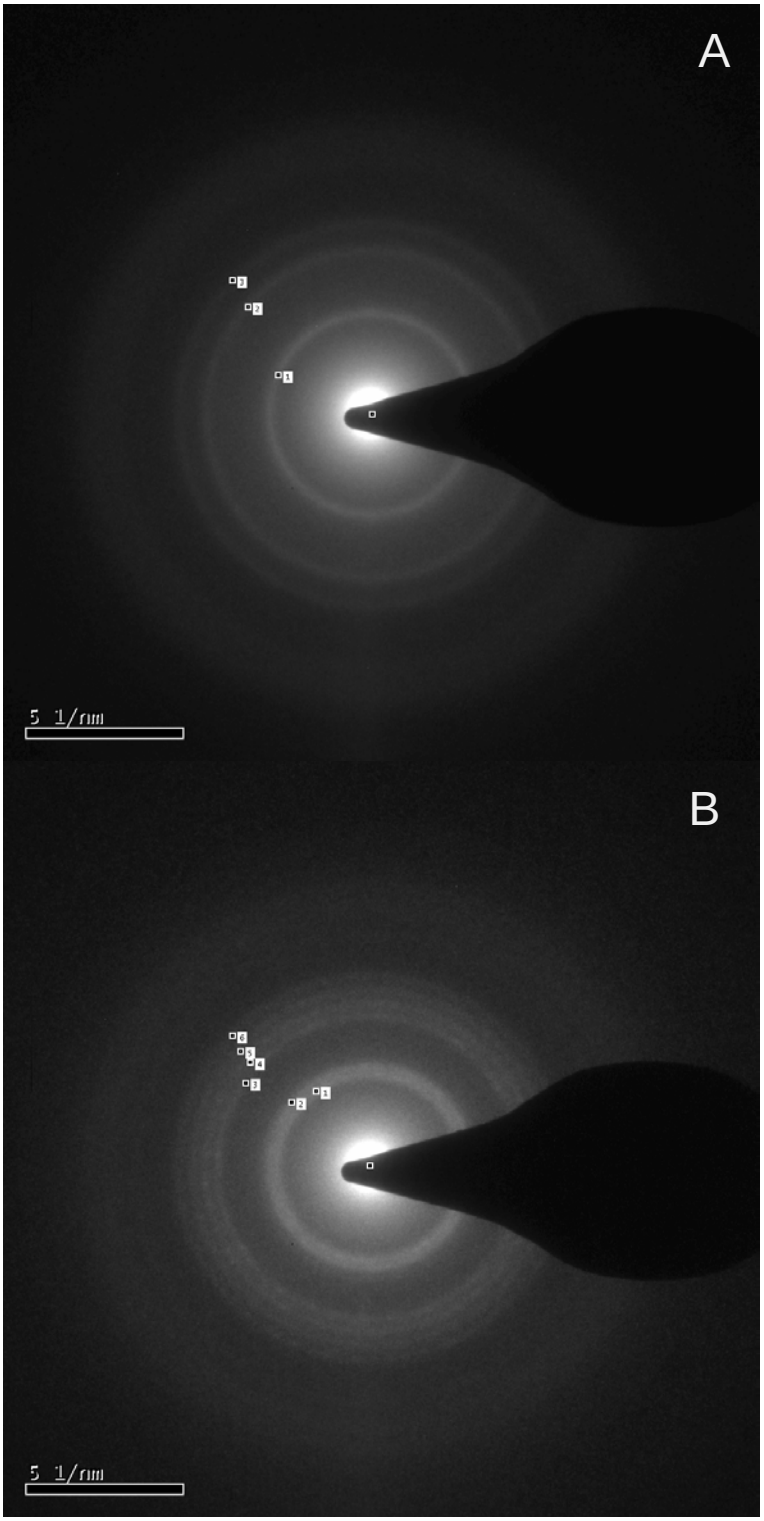

Figure 2. The SAED pattern of (A) pure CdS and (B) the structured CdS-ZnS.

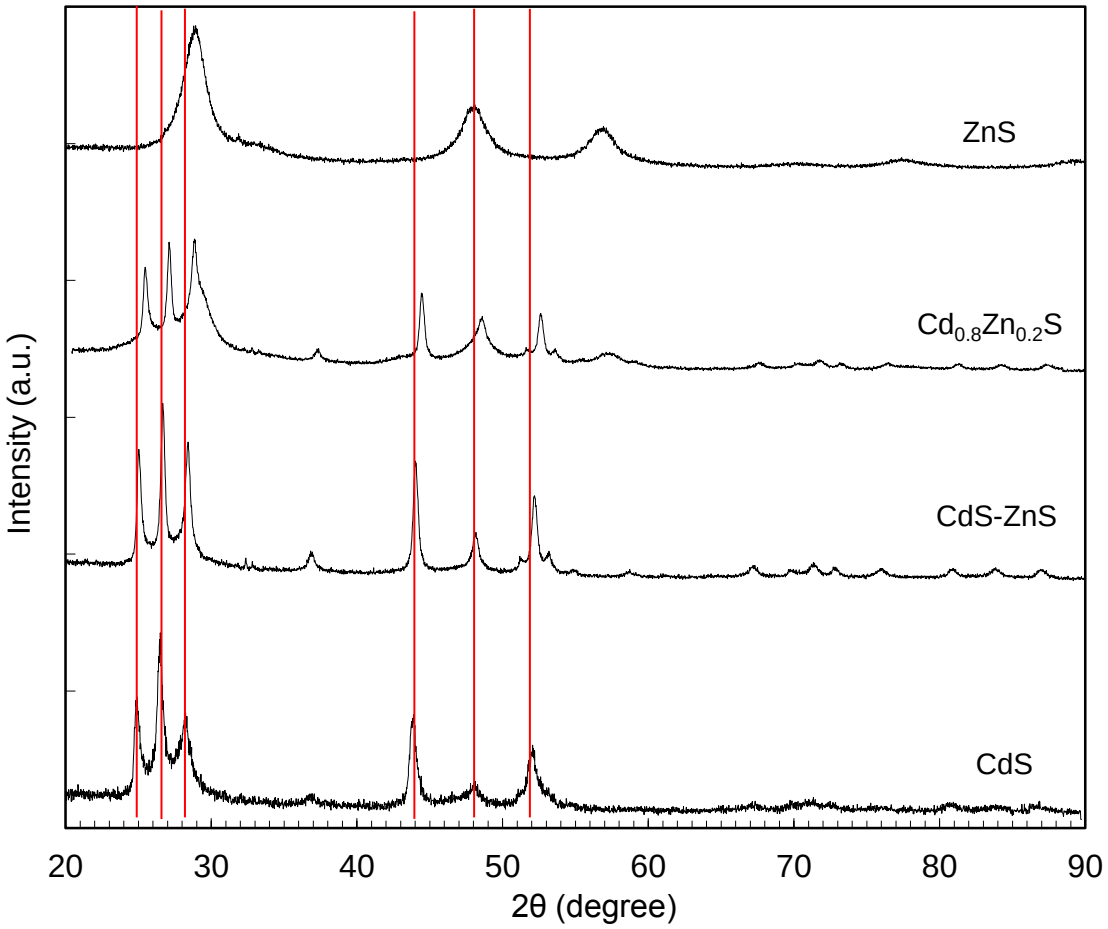

Figure 2. XRD spectra of the catalyst materials: the structured CdS-ZnS composite and pure CdS and ZnS.

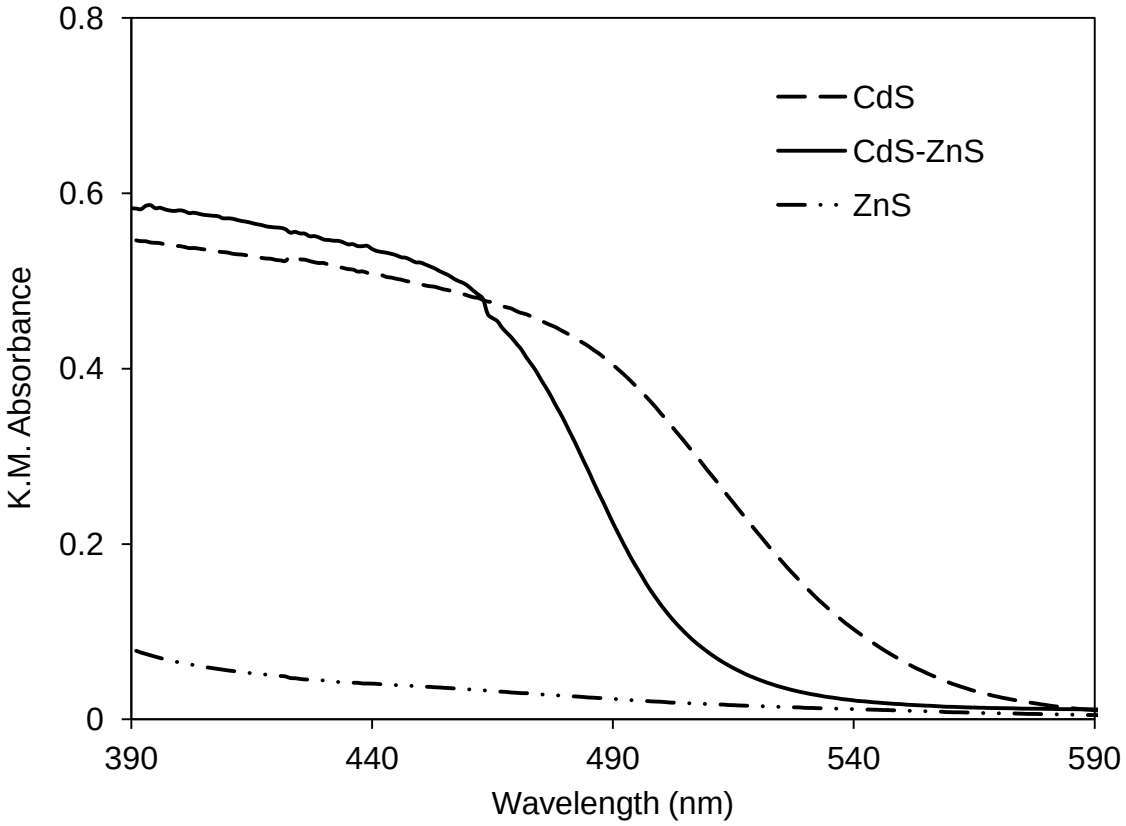

Figure 4. Diffuse reflection spectra of the photocatalysts: the structured CdS-ZnS composite in comparison with pure CdS and ZnS.

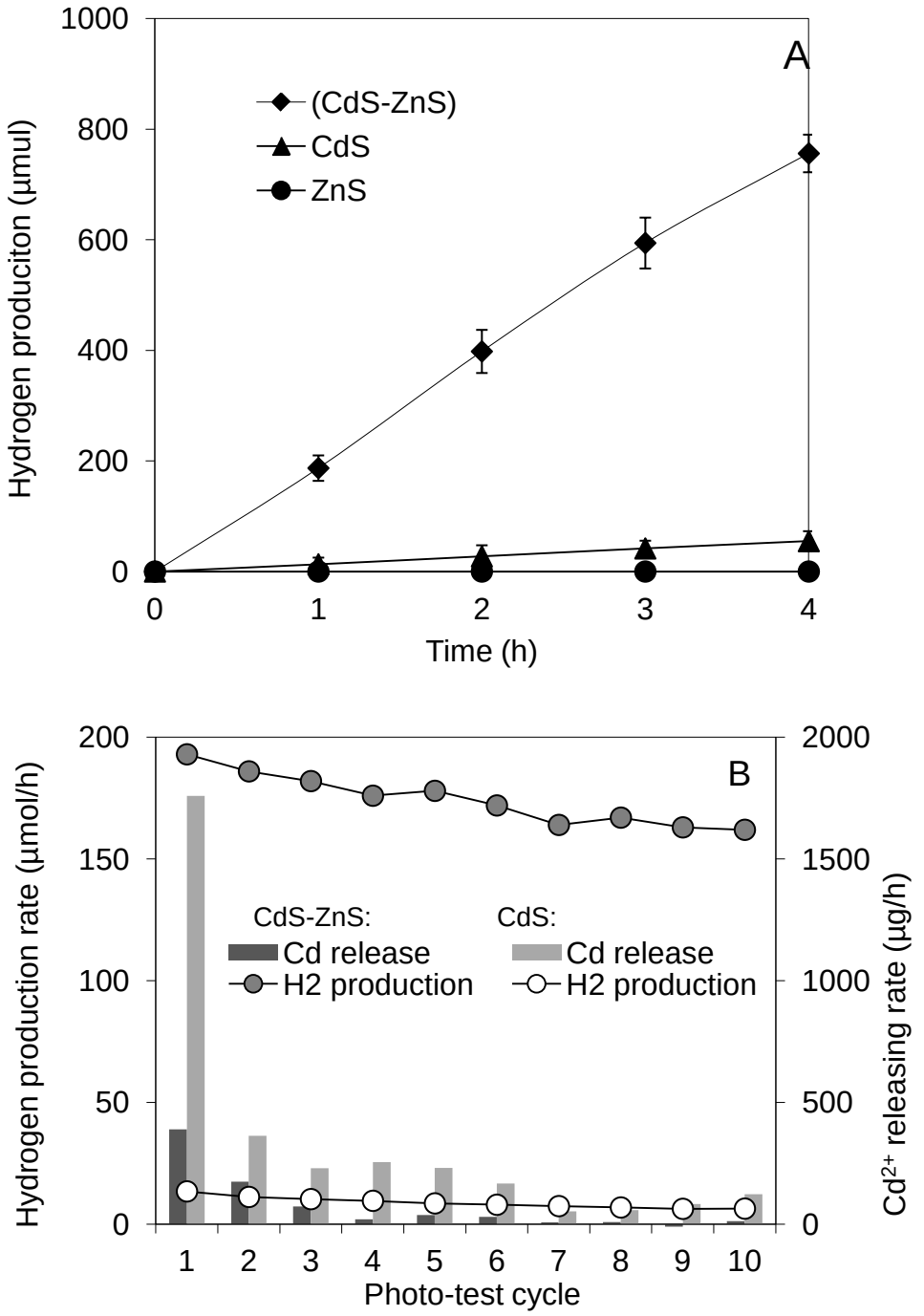

Figure 5. (A) Hydrogen production in the formic acid solution (10%) by the composite CdS-ZnS, bare CdS and bare ZnS, under visible light; and (B) stability of CdS-ZnS and bare CdS in terms of the hydrogen production rate and leaching of Cd^{2+} from the catalysts during the repeated photocatalytic tests (at least 4 hr for each test cycle).

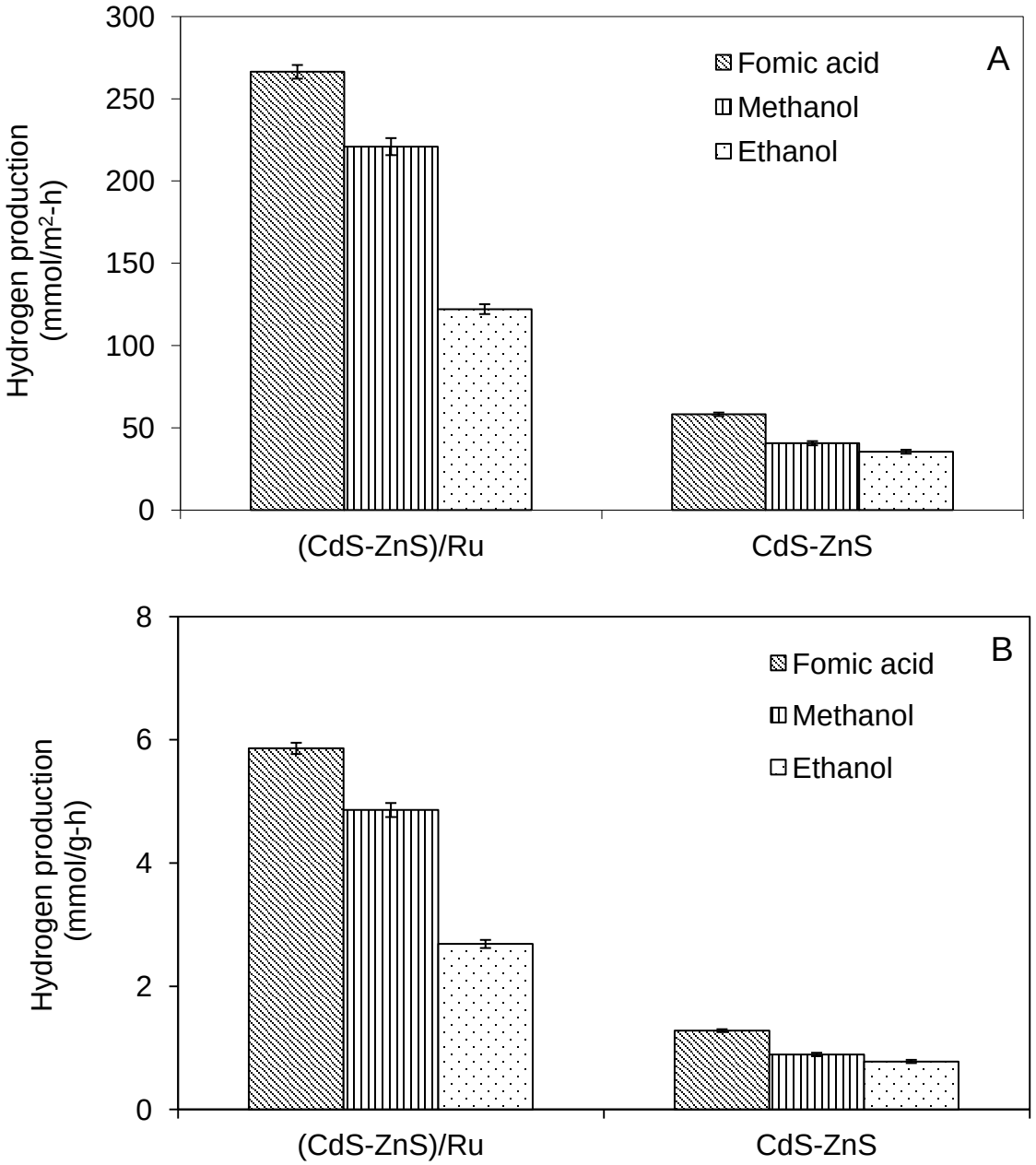

Figure 6. (A) The area-based and (B) weight-based specific hydrogen production rates of the photocatalysts of CdS-ZnS and (CdS-ZnS)/Ru in different model organic solutions (10%) under visible light.

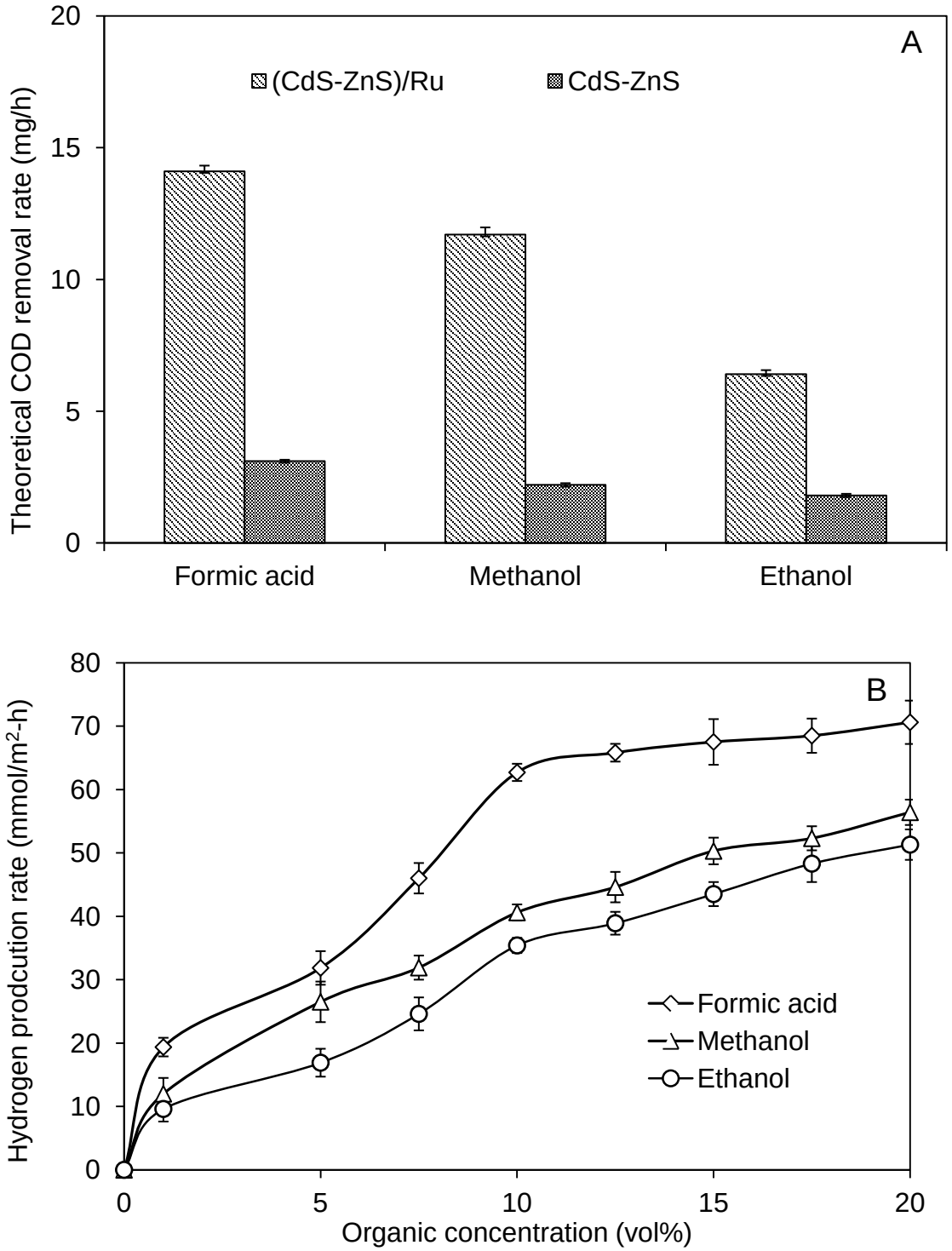

Figure 7. (A) The theoretical COD removal rate by the CdS-ZnS and (CdS-ZnS)/Ru photocatalysts for different organic solutions under visible light; and (B) the effect of the initial organic concentration on the rate of photocatalytic hydrogen production by CdS-ZnS under visible light.